

Hilbert statistics of vorticity scaling in two-dimensional turbulence

H. S. Tan(谭唤书),¹ Y. X. Huang(黄永祥),^{1,a)} and Jianping Meng(孟剑平)²

¹*Shanghai Institute of Applied Mathematics and Mechanics, Shanghai Key Laboratory of Mechanics in Energy Engineering, Shanghai University, Shanghai 200072, People's Republic of China*

²*Department of Mechanical and Aerospace Engineering, University of Strathclyde, Glasgow G1 1XJ, United Kingdom*

(Received 17 April 2013; accepted 18 December 2013; published online 13 January 2014)

In this paper, the scaling property of the inverse energy cascade and forward enstrophy cascade of the vorticity field $\omega(x, y)$ in two-dimensional (2D) turbulence is analyzed. This is accomplished by applying a Hilbert-based technique, namely Hilbert-Huang transform, to a vorticity field obtained from a 8192^2 grid-points direct numerical simulation of the 2D turbulence with a forcing scale $k_f = 100$ and an Ekman friction. The measured joint probability density function $p(C, k)$ of mode $C_i(x)$ of the vorticity ω and instantaneous wavenumber $k(x)$ is separated by the forcing scale k_f into two parts, which correspond to the inverse energy cascade and the forward enstrophy cascade. It is found that all conditional probability density function $p(C|k)$ at given wavenumber k has an exponential tail. In the inverse energy cascade, the shape of $p(C|k)$ does collapse with each other, indicating a nonintermittent cascade. The measured scaling exponent $\zeta_\omega^I(q)$ is linear with the statistical order q , i.e., $\zeta_\omega^I(q) = -q/3$, confirming the nonintermittent cascade process. In the forward enstrophy cascade, the core part of $p(C|k)$ is changing with wavenumber k , indicating an intermittent forward cascade. The measured scaling exponent $\zeta_\omega^F(q)$ is nonlinear with q and can be described very well by a log-Poisson fitting: $\zeta_\omega^F(q) = \frac{1}{3}q + 0.45(1 - 0.43^q)$. However, the extracted vorticity scaling exponents $\zeta_\omega(q)$ for both inverse energy cascade and forward enstrophy cascade are not consistent with Kraichnan's theory prediction. New theory for the vorticity field in 2D turbulence is required to interpret the observed scaling behavior. © 2014 AIP Publishing LLC. [<http://dx.doi.org/10.1063/1.4861068>]

I. INTRODUCTION

Two-dimensional (2D) turbulence is an ideal model for several turbulent phenomena, such as the first approximation to the large-scale motion in atmosphere and oceans.¹⁻⁵ The 2D turbulence and relative problems have attracted a lot of attentions in recent years.⁶⁻¹⁸ Several review papers have been devoted to this topic in detail, for example, papers by Tabeling,² Kellay and Goldburg,³ Boffetta and Ecke,⁴ Bouchet and Venaille,⁵ Van Heijst and Clercx,¹⁹ to quote a few. The 2D Ekman-Navier-Stokes equation is written in terms of a single scalar vorticity field $\omega = \nabla \times \mathbf{u}$ as, i.e.,

$$\partial_t \omega + \mathbf{u} \bullet \nabla \omega = \nu \nabla^2 \omega - \alpha \omega + f_\omega, \quad (1)$$

in which ν is the fluid viscosity, α is the Ekman friction, and f_ω is an external source of energy inputting into the whole system.^{20,21} Specifically for the small scale motions, it is believed that there exists a dual-cascade, i.e., a forward enstrophy cascade, in which the enstrophy (square of vorticity ω^2) is transferred from large to small scales, and an inverse energy cascade, in which the energy is

^{a)}Electronic mail: yongxianghuang@gmail.com

transferred from small to large scales.²² A two-power-law behavior is thus expected to describe this dual cascade, i.e.,

$$E_u(k) = \begin{cases} C (\epsilon_\alpha)^{2/3} k^{-5/3}, & \text{when } k_\alpha \ll k \ll k_f \text{ for inverse energy cascade} \\ C' (\eta_v)^{2/3} k^{-3}, & \text{when } k_f \ll k \ll k_v \text{ for forward enstrophy cascade} \end{cases}, \quad (2)$$

in which $E_u(k)$ is the Fourier power spectrum of the velocity, ϵ_α is the energy dissipation by the Ekman friction, η_v is the enstrophy dissipation by the viscosity, k_f is the forcing scale, in which the energy and enstrophy is injected into the system, k_α is the characteristic friction scale, and k_v is the viscosity scale. One can relate the vorticity statistics with the velocity one by using $E_\omega(k) \sim k^2 E_u(k)$. Therefore, a dual power-law behavior is also expected for the vorticity field, i.e.,

$$E_\omega(k) \sim k^2 E_u(k) \sim \begin{cases} k^{1/3}, & \text{when } k_\alpha \ll k \ll k_f \text{ for inverse energy cascade} \\ k^{-1}, & \text{when } k_f \ll k \ll k_v \text{ for forward enstrophy cascade} \end{cases}. \quad (3)$$

It is found experimentally that the probability density function (pdf) of the velocity increment $\Delta_\ell u$ is Gaussian when the separation scale ℓ lies in the inverse energy cascade, indicating nonintermittent behavior on these scales.^{2-5,19} Note that the classical structure-function (SF) analysis fails when the slope β of the Fourier power spectrum is out of the range $1 < \beta < 3$, in which $E(k) \sim k^{-\beta}$.^{23,24} This unfortunately is the case of the forward enstrophy cascade in the 2D turbulence.^{4,25} Therefore, the intermittent property of the forward enstrophy cascade cannot be verified directly by using the SF analysis.^{20,25} Kellay, Wu, and Goldburg²⁶ performed an experimental measurement of the velocity and vorticity field of the 2D soap turbulence. They found that the Fourier power spectrum of the velocity shows a -3 power-law for the forward enstrophy cascade, which agrees very well with the theory. However, the corresponding Fourier power spectrum of the vorticity field for the forward enstrophy cascade demonstrates a -2 power-law, which is contradicted with the theoretical prediction, see Eq. (3). For the velocity measurement, Paret, Jullien, and Tabeling²⁷ also observed -3 scaling for the forward enstrophy cascade. Moreover, the measured pdf of vorticity increment $\Delta_\ell \omega$ is not significant deviation from the Gaussian distribution, i.e., a nonintermittent forward enstrophy cascade. On the contrary, Nam *et al.*²⁸ found that if an Ekman friction coefficient α is presented, the forward enstrophy cascade is then intermittent.²⁹ Boffetta *et al.*²⁰ argued that if a passive scalar θ is governed by the same equation as the vorticity field and if it is also advected by the same velocity field, it then can be taken as a surrogate of the vorticity ω for the small scale statistics. They found that the passive scalar θ is indeed intermittent. Moreover, they found that the fitting scaling exponent for the forward enstrophy cascade is dependent on the Enkman viscosity α . Later, Tsang *et al.*³⁰ studied the intermittency of the forward enstrophy cascade regime with a linear drag. The relative scaling exponent ($\zeta(2q)/\zeta(2)$) provided by the vorticity SF confirms that the forward enstrophy cascade is intermittent for the considered statistical order $0 \leq q \leq 2$. Note that the classical SF approach is employed in their studies. Biferale *et al.*²⁵ proposed an inverse velocity statistics and applied in 2D turbulence. They found that the velocity fluctuation cannot be simply described by one single exponent, indicating an intermittent forward cascade. Boffetta²¹ reported that the fitting scaling exponent of the Fourier power spectrum for the forward cascade might also depend on the viscosity ν . Recently, Falkovich and Lebedev³¹ derived analytically the probability density function for strong vorticity fluctuations (respectively the tail of the pdf) in the forward enstrophy cascade. They found that the over R coarse-grained vorticity $\overline{\omega}(R)$ has a universal asymptotic exponential tail and is thus self-similar without intermittency (respectively scaling exponent is linear with q) at least for high-order statistics. Generally speaking, Kraichnan's theory of 2D turbulence is partially confirmed by the experiments and numerical simulation for the velocity field.³² However, as mentioned above, the statistics of the vorticity field seems to disagree with the theoretical prediction.

In this paper, we apply a Hilbert-based technique to the vorticity $\omega(x, y)$ field obtained from a high resolution direct numerical simulation (DNS). A dual-cascade behavior is observed, respectively, with a nearly one decade inverse energy cascade and forward enstrophy cascade. For the inverse energy cascade, the measured vorticity pdf does collapse with each other, implying a nonintermittent cascade process as expected.^{4,5,31} The corresponding measured scaling exponent $\zeta_\omega^I(q)$ is linear with q , i.e., $\zeta_\omega^I = q/3$. For the forward enstrophy cascade, the measured vorticity pdf possesses an

exponential tail, which is consistent with the findings in Ref. 31. However, they cannot collapse with each other, indicating an intermittent forward enstrophy cascade. The measured scaling exponent $\zeta_\omega^F(q)$ is nonlinear with a small q and asymptotic to a linear relation for large q . A log-Poisson-like formula is proposed to describe the measured scaling exponent, i.e., $\zeta_\omega^F = q/3 + 0.45(1 - 0.43^q)$ for the forward enstrophy cascade. Note that for the vorticity field, the measured scaling exponents disagree with the theoretical prediction by Kraichnan²² even one takes the logarithmic correction into account. New theory about the vorticity field is required to interpret our findings in this work.

II. HILBERT-HUANG TRANSFORM

A. Empirical mode decomposition

The method we used in this work is the so-called arbitrary-order Hilbert spectral analysis.^{33,34} It is an extended version of the Hilbert-Huang Transform (HHT).^{35,36} The Hilbert method contains two steps. In the first step, a data-driven algorithm, namely Empirical Mode Decomposition (EMD), is designed to decompose a given signal, e.g., $\omega(x)$, into a sum of Intrinsic Mode Functions (IMFs) $C_i(x)$ without *a priori* basis.^{35,37} The IMF is an approximation of the mono-component signal, which has to satisfy the following two conditions: (i) the difference between the number of local extrema and the number of zero-crossings must be zero or one; (ii) the running mean value of the envelope defined by the local maxima and the envelope defined by the local minima is zero.^{35,36,38} The extracted IMF mode possesses a well-behaved Hilbert spectrum with a physical meaningful instantaneous frequency in time domain (respectively wavenumber in space domain).^{35,36} Figure 1 shows a flowchart of the EMD algorithm to demonstrate how to decompose a given vortex signal $\omega(x)$ into a sum of IMF modes, i.e.,

$$\omega(x) = \sum_{i=1}^N C_i(x) + r_N(x), \quad (4)$$

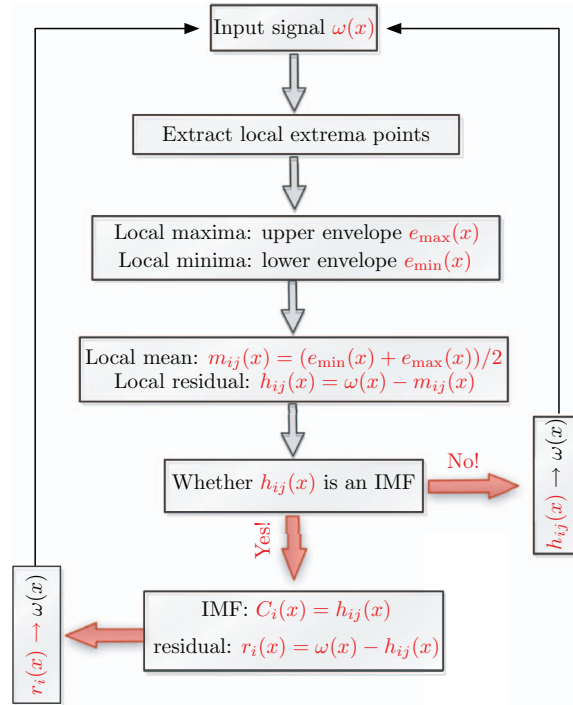


FIG. 1. A flowchart of the empirical mode decomposition algorithm to show how to decompose a given vortex field $\omega(x, y)$ at certain y into a sum of intrinsic mode functions $C_i(x)$.

in which $r_N(x)$ is residual. There exist several criteria to stop the sifting process and to determine whether an IMF mode is retrieved.^{35,36,38} For example, Huang *et al.*³⁵ have proposed a Cauchy like criteria computed from two consecutive sifting, i.e.,

$$SD = \frac{\int [h_{i(j-1)}(x) - h_{ij}(x)]^2 dx}{\int [h_{i(j-1)}(x)]^2 dx}, \quad (5)$$

in which $h_{ij}(x)$ is the residual by removing the running mean $m_{ij}(x)$ constructed by using upper $e_{\max}(x)$ and lower envelopes $e_{\min}(x)$. Here $e_{\max}(x)$ (respectively $e_{\min}(x)$) is the upper envelope constructed by using the local maxima points (respectively minima points). A typical value can be set between 0.2 and 0.3 to provide a physical meaningful IMF mode. Another widely used stopping criteria is proposed by Rilling, Flandrin, and Gonçalves.³⁸ They introduced an amplitude function $a(x) = (e_{\max}(x) - e_{\min}(x))/2$ and an evaluation function $\sigma(x) = m_{ij}(x)/a(x)$, respectively. The sifting procedure is iterated until $\sigma(x) < \theta_1$ for some prescribed fraction $(1 - \alpha)$ of the total data, while $\sigma(x) < \theta_2$ for the rest fraction. Typical values are $\alpha \simeq 0.05$, $\theta_1 \simeq 0.05$, and $\theta_2 \simeq 10\theta_1$.³⁸ A maximum iteration number, i.e., 100, could also be used to stop the sifting. In our practice, any one of the above three criteria is satisfied, then one IMF mode is retrieved.

B. Hilbert spectral analysis

After retrieving the IMF modes, the Hilbert spectral analysis is applied to each mode to obtain the time-frequency information.^{35,36,39} The Hilbert transform is defined as, i.e.,

$$\bar{C}_i(x) = \frac{1}{\pi} P \int \frac{C_i(x')}{x - x'} dx', \quad (6)$$

in which P means the Cauchy principle value.^{40,41} A so-called analytical signal is then written as, i.e.,

$$C_i^A(x) = C_i(x) + j\bar{C}_i(x), \quad (7)$$

in which $j = \sqrt{-1}$. An instantaneous wavenumber is then defined as, i.e.,

$$k_i(x) = \frac{1}{2\pi} \frac{d}{dx} \arctan \left(\frac{\bar{C}_i(x)}{C_i(x)} \right). \quad (8)$$

Note that Eq. (6) is a singularity transform. The differential operation is also used to define the instantaneous wavenumber, see Eq. (8). Therefore, the Hilbert method possesses a very local ability in the wavenumber domain. The final representation of the original data $\omega(x)$ can be written as, i.e.,

$$\omega(x) = \sum_{i=1}^N \mathcal{A}_i(x) \exp \left(\int_{-\infty}^x j k_i(x') dx' \right), \quad (9)$$

in which $\mathcal{A}_i(x) = \sqrt{\bar{C}_i(x)^2 + C_i(x)^2}$ is the modulus of $C_i^A(x)$.^{34,35} Comparison with the Fourier analysis, the above representation can be considered as a local Fourier expansion, in which the amplitude \mathcal{A} and wavenumber k can be varied with x , namely amplitude, and frequency-modulation.³⁵

C. Arbitrary order Hilbert spectral analysis

After obtaining the IMF modes $C_i(x)$ and the corresponding instantaneous wavenumber $k_i(x)$, one can construct a set of pair $[C_i(x), k_i(x)]$. A k -conditional q th-order statistical moment is then defined as, i.e.,

$$\mathcal{L}_q(k) = \left\langle \sum_{i=1}^N [C_i(x)]_{k_i(x)=k}^q \right\rangle_x, \quad (10)$$

in which $\langle \dots \rangle$ is ensemble average over all i and x .^{34,42} $\mathcal{L}_q(k)$ could be defined by another equivalent way as described below. One can extract a joint probability density function (pdf), i.e., $p(C, k)$,

from the IMF mode $C_i(x)$ and the corresponding wavenumber $k_i(x)$. Taking a marginal integration, Eq. (10) is then rewritten as, i.e.,

$$\mathcal{L}_q(k) = \frac{\int p(C, k) |C|^q dC}{\int p(C, k) dC}. \quad (11)$$

For a scaling process, one expects a power-law behavior, i.e.,

$$\mathcal{L}_q(k) \sim k^{-\zeta(q)}, \quad (12)$$

in which $\zeta(q)$ is comparable with the scaling exponents provided by the classical structure function.³⁴

The Hilbert-based methodology has been verified by using a synthesized fractional Brownian motion data for mono-fractal process and a synthesized multifractal random walk with a lognormal statistics for multifractal process.³⁴ It also has been applied successfully to turbulent velocity,³³ passive scalar,²⁴ Lagrangian turbulence,⁴² etc., to characterize the intermittent nature of those processes. Our experience is that the SF analysis works when $1 < \beta < 3$ without energetic structures.²⁴ Here β is the scaling exponent of Fourier power spectrum, i.e., $E(k) \sim k^{-\beta}$. If β is out of this range, then the Hilbert methodology should be applied to extract scaling exponents for high-order q . Moreover, due to the influence of energetic structures, the SFs may fail even when $\beta = 2$. This has been found to be the case of the three-dimensional Lagrangian turbulence.⁴² We will show below that this is also the case of 2D turbulence, see more discussion in Sec. III B. For more detail about the methodology we refer the reader to the Refs. 33–35, 39, and 42.

III. NUMERICAL DATA AND SCALING OF HIGH-ORDER STATISTICS

A. Direct numerical simulation of 2D turbulence

The DNS data we used in this study are provided by Professor Boffetta. We recall briefly several key parameters of this simulation. Numerical integration of Eq. (1) is performed by a pseudo-spectral, fully dealiased on a doubly periodic square domain of size $L = 2\pi$ at resolution $N^2 = 8192^2$ grid points.²¹ The main parameters are, respectively, $\nu = 2 \times 10^{-6}$, $\alpha = 0.025$, and $k_f = 100$, in which the energy is inputted into the system. The velocity field $\mathbf{u} = \nabla \times \Phi$ is then obtained by solving a Poisson problem $\nabla^2 \Phi = -\omega$, in which Φ is a stream function. Totally, we have five snapshots with $8192^2 \times 5 = 3.36 \times 10^8$ data points. In the following, the analysis is done along the x -direction. This provides $8192 \times 5 = 40\,960$ realizations for each statistics. The ensemble average is then averaged from all these realizations. Figure 2 shows a portion of one snapshot of the vorticity field. Note that high intensity events are discretely distributed in physical space with a typical wavenumber $k \simeq k_f = 100$ (respectively ~ 80 grid points). More details of this database can be found in Ref. 21.

B. Fourier power spectrum and second-order structure-function

Figure 3(a) shows the measured Fourier power spectrum $E_\omega(k)$ (solid line) of the vorticity field, in which the logarithmic correction $E_\omega(k) \ln(k/k_{\min})^{-1/3}$ is shown as a dashed line. A power-law behavior for the forward enstrophy cascade is observed on the range $100 \leq k \leq 1000$, i.e., $E_\omega(k) \sim k^{-\beta}$, with a scaling exponent $\beta = 1.96 \pm 0.02$. The measured β is consisted with the one reported by Kellay, Wu, and Goldburg.²⁶ The observed scaling range corresponds to a spatial scale range $0.001 \leq \ell \leq 0.01$. The logarithmic correction provides a scaling exponent $\beta = 2.02 \pm 0.02$ on the same scaling range, showing a weak correction of the power-law behavior.⁴³ The inset shows the corresponding compensated curves to emphasize the observed power-law behavior. We therefore expect a power-law behavior on the range $0.001 \leq \ell \leq 0.01$ for the second-order SFs, i.e.,

$$S_\omega(2, \ell) = \langle |\Delta_\ell \omega|^2 \rangle \sim \ell^{\beta-1}, \quad (13)$$

in which $\Delta_\ell \omega = \omega(x + \ell) - \omega(x)$ is vorticity increment, and β is the scaling exponent from $E_\omega(k) \sim k^{-\beta}$. Figure 3(b) shows the measured second-order SF, in which the forward enstrophy cascade is illustrated by a vertical solid line. Visually, no power-law behavior is observed for the measured $S_\omega(2, \ell)$ for the forward enstrophy cascade. To emphasize this point, the local slope, i.e.,

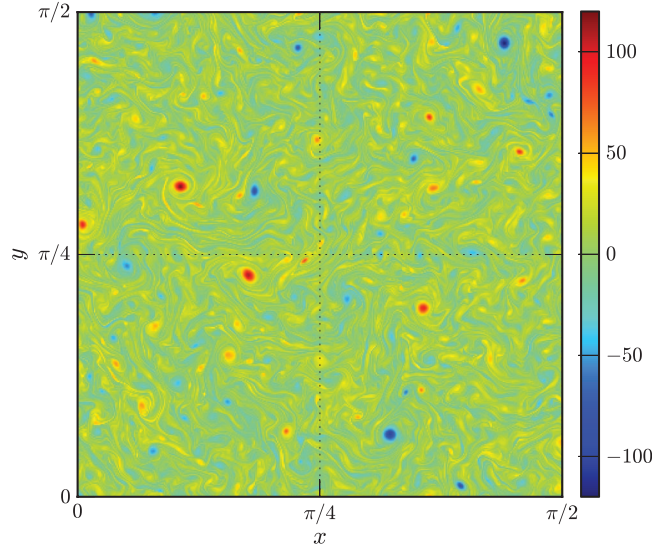


FIG. 2. A snapshot of the vorticity field $\omega(x, y)$ of the two-dimensional turbulence on the range $0 \leq x, y \leq \pi/2$ from a high resolution direct numerical simulation with 8192^2 grid points. High intensity vorticity events are discrete distributed in space with a typical wavenumber $k \simeq k_f = 100$ (respectively around 80 grid points).

$\zeta_\omega(2, \ell) = \text{dlog}_{10} S_\omega(2, \ell) / \text{dlog}_{10} \ell$, is shown in the inset. There is no plateau observed on the range of the forward enstrophy cascade, showing the failure of the SFs to capture the scale invariance of the two-dimensional vorticity field.

To understand more about the second-order SFs $S_\omega(2, \ell)$, one can relate it with the Fourier power spectrum by using Wiener-Khinchin theorem,^{23,24} i.e.,

$$S_\omega(2, \ell) = \int_0^{+\infty} E_\omega(k) (1 - \cos(2\pi k \ell)) dk, \quad (14)$$

in which $E_\omega(k)$ is the corresponding Fourier power spectrum. Note that an integral constant is neglected since it does not change the conclusion in this paper. The above equation implies that the SFs contain contribution from almost all Fourier modes k . The expected power-law behavior might be influenced by both large-scale (respectively low wavenumber, known as infrared effect, IR)

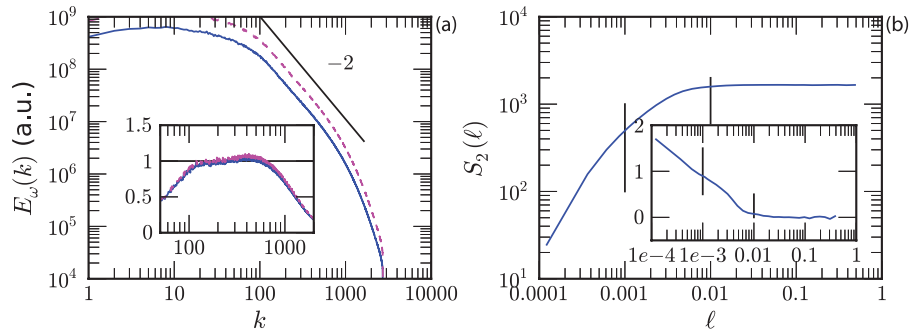


FIG. 3. (a) Measured Fourier power spectrum $E_\omega(k)$ for vorticity field $\omega(x, y)$, in which a logarithmic correction $E_\omega(k) \ln(k/k_{\min})^{-1/3}$ is shown as a dashed line. For display clarity, the measured $E_\omega(k) \ln(k/k_{\min})^{-1/3}$ has been vertically shifted by multiplying a factor 5. A nearly one decade power-law behavior is found on the wavenumber range $100 \leq k \leq 1000$, corresponding to $0.001 \leq \ell \leq 0.01$ with a scaling exponent $\beta = 1.96 \pm 0.02$ for $E_\omega(k)$ and $\beta = 2.02 \pm 0.02$ for $E_\omega(k) \ln(k/k_{\min})^{-1/3}$, respectively. The inset shows the compensated spectrum with fitted scaling exponents. This scaling range corresponds to the forward enstrophy cascade. (b) Measured second-order structure-function $S_\omega(2, \ell)$. No power-law behavior is observed as expected on the range $0.001 \leq \ell \leq 0.01$. The inset shows the local slope $\zeta_\omega(2, \ell) = \text{dlog}_{10} S_\omega(2, \ell) / \text{dlog}_{10} \ell$ to confirming the lacking of the power-law behavior.

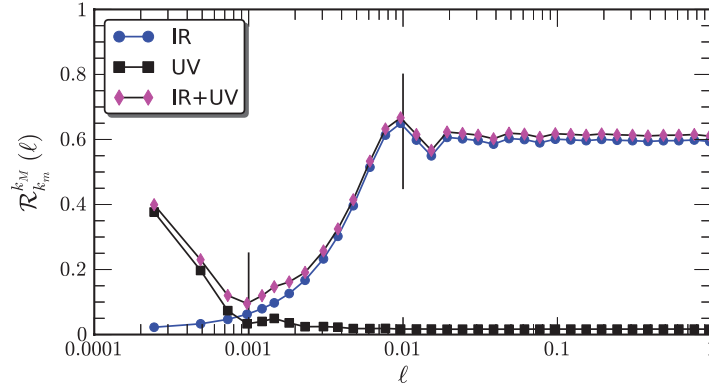


FIG. 4. Measured relative contribution function $\mathcal{R}_{k_m}^{k_M}(\ell)$ from different Fourier modes. Low wavenumber part (IR) $[0, 100]$ (\circ), high wavenumber part (UV) $[1000, +\infty]$ (\square). The expected power-law range is illustrated by a vertical solid line. Note that the expected power-law behavior is strongly influenced by the low wavenumber part, known as IR effect.

and small-scale (respectively high wavenumber, known as ultraviolet effect, UV) motions. A partial cumulative function is therefore introduced to characterize a relative contribution from Fourier modes band $[k_m, k_M]$, i.e.,

$$\mathcal{R}_{k_m}^{k_M}(\ell) = \frac{\int_{k_m}^{k_M} E_\omega(k')(1 - \cos(2\pi k' \ell)) dk'}{\int_0^{+\infty} E_\omega(k)(1 - \cos(2\pi k \ell)) dk}. \quad (15)$$

We are particular concerned by the Fourier modes below the forcing scale, i.e., $[0, 100]$ (respectively IR) and by the modes above the power-law range, i.e., $[1000, +\infty]$ (respectively UV). Figure 4 shows the measured $\mathcal{R}_m^M(\ell)$ for IR (\circ) and UV (\square). It indicates that the SFs are strongly influenced by the large-scale motions (respectively IR) as high as up to 65%. The expected power-law behavior is then destroyed.^{24,44}

We provide some comments on the above analysis here. The Wiener-Khinchin theorem is only exactly valid for the linear and stationary processes. Turbulent signals in 3D or 2D are typical non-linear and nonstationary ones. Therefore, the above argument holds approximately here. However, this does not change the conclusion of this paper. Another comment is for the observed high intensity vorticity event, see Fig. 2. For the high-order SFs, they might be also influenced by those events since they usually manifest themselves at the pdf tail of vorticity increments. This has been observed for the Lagrangian turbulence, in which the high intensity event is known as “vortex trapping” process.^{42,45}

C. Generalization scaling for high-order statistics

Assuming that we have SFs scaling for both the inverse and forward cascades. The corresponding SFs and their scaling exponents without intermittent corrections are

$$S_u(q, \ell) \sim \begin{cases} \ell^{q/3}, & \text{for inverse energy cascade} \\ \ell^q, & \text{for forward enstrophy cascade} \end{cases}, \quad (16a)$$

for the velocity field,⁷ and

$$S_\omega(q, \ell) \sim \ell^{-q} S_u(q, \ell) \sim \begin{cases} \ell^{-2q/3}, & \text{for inverse energy cascade} \\ \ell^0, & \text{for forward enstrophy cascade} \end{cases}, \quad (16b)$$

for the vorticity field. It implies that the forward enstrophy cascade represented by the vorticity field is independent on the separation scale ℓ . In the frame of Hilbert, we expect the following scaling behavior for the vorticity field, i.e.,

$$\mathcal{L}_\omega(q, k) \sim \begin{cases} k^{2q/3}, & \text{for inverse energy cascade} \\ k^0, & \text{for forward enstrophy cascade} \end{cases}. \quad (16c)$$

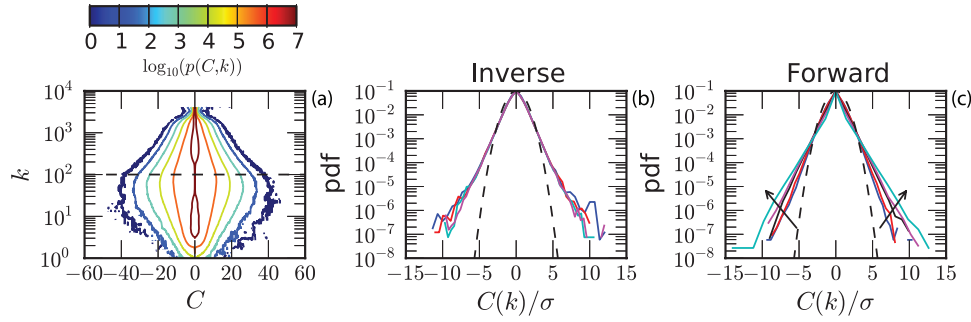


FIG. 5. (a) Contour plot of measured conditional histogram $p(C, k)$ (respectively joint probability density function (pdf)), in which the force scale is illustrated by a dashed line. (b) Measured pdf $p(C)$ on the range $3 < k < 20$ (respectively $k = 4, 6, 16$, and 20) for the inverse energy cascade. (c) Measured pdf $p(C)$ on the range $200 < k < 2000$ (respectively $k = 250, 400, 800, 1000$, and 1600) for the forward enstrophy cascade. For comparison, the normal distribution is illustrated by a dashed line.

We will then test above relation by using the Hilbert method as we described above.

IV. HILBERT RESULTS AND DISCUSSION

A. Hilbert statistics

The Hilbert method is applied to the vorticity field $\omega(x, y)$ along x -direction. The conditioned/joint histogram $p(C, k)$ (respectively probability density function if it is renormalized properly) is extracted from all five snapshots. Figure 5(a) shows the contour plot of the measured $p(C, k)$, in which the forcing scale $k_f = 100$ is illustrated by a horizontal dashed line. For display clarity, we take the logarithm of the measured $p(C, k)$. It is interesting to note that the joint pdf is roughly separated by the forcing wavenumber $k_f = 100$ into two regimes. The first regime is on the range $2 \leq k \leq 20$, corresponding to the inverse energy cascade. The another one is on the range $200 \leq k \leq 2000$, corresponding to the forward enstrophy cascade. Figure 5(b) shows the pdf $p(C|k)$ on the inverse energy cascade (respectively $k = 4, 6, 16$, and 20). For comparison, the normal distribution is demonstrated by a solid line. All the measured pdf has an exponential tail. We note that the pdf in the inverse energy cascade does collapse with each other, indicating a nonintermittent cascade. For the pdf in the forward enstrophy cascade, they also possess an exponential tail. However, they cannot collapse with each other due to different shape of the core part $-5 < C(k)/\sigma < 5$. The exponential tail of the vorticity field consists with very recently theoretical prediction by Falkovich and Lebedev.³¹

Figure 6 shows the comparison of the measured Hilbert energy spectrum $\mathcal{L}_2(k)/k$ (\square) and the Fourier power spectrum $E_\omega(k)$ (solid line). For display clarity, the curve has been vertically shifted. Note that both methods provide the nearly same forward enstrophy cascade on the range $100 < k < 1000$ with a scaling exponent close to $\simeq 2$. This scaling exponent agrees very well with the experimental observation by Kellay, Wu, and Goldburg.²⁶ We show in the inset the compensated curve by using the fitted exponent for the forward cascade (closed square for the Hilbert and solid line for Fourier). The observed plateau confirms the power-law behavior as expected. Furthermore, we have an additional power-law behavior on the range $3 < k < 20$ for the inverse energy cascade. The compensated spectra are also shown in the inset (open square for the Hilbert and dashed line for Fourier) to emphasize the observed inverse energy cascade. Both Hilbert and Fourier methodologies identify almost the same dual power-law behavior.

We now turn to the high-order Hilbert statistics. The convergence of the statistical moment $\mathcal{L}_q(k)$ has been verified by checking the integral kernel $p(C, k)|C|^q$ at given scales. A quite good convergence has been found for all wavenumber k up to $q = 4$ (not shown here). Figure 7(a) shows the measured $\mathcal{L}_q(k)$ for $q = 1, 2, 3$, and 4 (from bottom to top). A dual power-law behavior is observed as expected, respectively, on the range $3 \leq k \leq 20$ for the inverse energy cascade and $200 \leq k \leq 2000$ for the forward enstrophy cascade. The scaling exponent $\zeta_\omega(q)$ is then estimated,

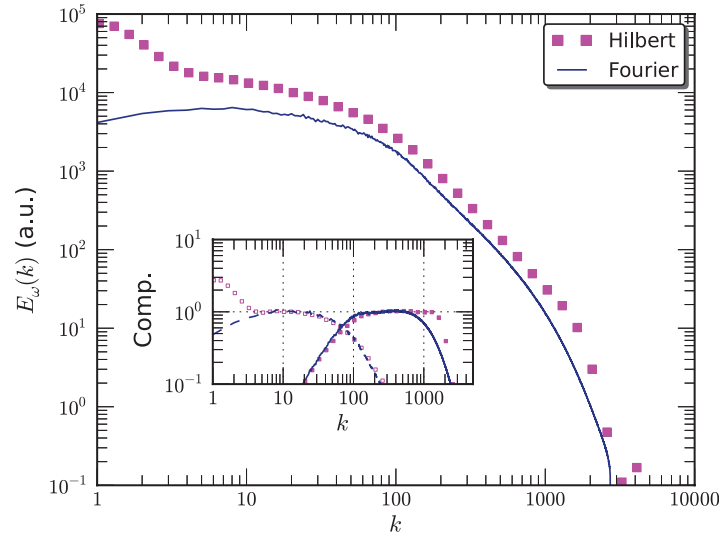


FIG. 6. Comparison of the measured Hilbert energy spectrum $\mathcal{L}_2(k)/k$ (\square) and the Fourier energy spectrum $E_\omega(k)$ (solid line). For display clarity, the curves have been vertically shifted. Inset shows the corresponding compensated spectra for both inverse energy cascade and forward enstrophy cascade by using fitting scaling exponents, respectively, on the range $3 < k < 20$ and $100 < k < 1000$.

respectively, on these two ranges by using a least square fitting algorithm. Figure 7(b) shows the corresponding measured scaling exponent $\zeta_\omega(q)$, in which the errorbar is 95% fitting confidence. For the inverse energy cascade, the measured $\zeta_\omega^I(q)$ (\square) is linear with q , i.e., $\zeta_\omega^I(q) = -q/3$, confirming that there is no intermittent effect in this inverse cascade process.⁴ However, the observed $-q/3$ scaling does not agree with the prediction of Eq. (16c). This implies that for the vorticity field some important mechanisms are ignored in the previously dimensional arguments of the inverse energy cascade. For example, if one takes the enstrophy dissipation η_α into account and assumes it as important as the Ekman energy dissipation ϵ_α , one then has the right scaling behavior, i.e., $\mathcal{L}_q(k) \sim (\epsilon_\alpha \eta_\alpha)^{q/6} k^{q/3}$. This corresponds to a scaling exponent $\zeta_\omega^I(q) = -q/3$ for the inverse energy cascade. However, this naive dimensional argument should be justified for physical evidence and for more database.

The measured scaling exponent $\zeta_\omega^F(q)$ (\circ) is also shown in Fig. 7(b). We note that when $q \leq 2$ the measured $\zeta_\omega^F(q)$ is nonlinear dependent with q , indicating an intermittent effect of the vorticity field. While when $q \geq 2$, it seems to be linear with q with a slope $\simeq 1/3$. We propose here

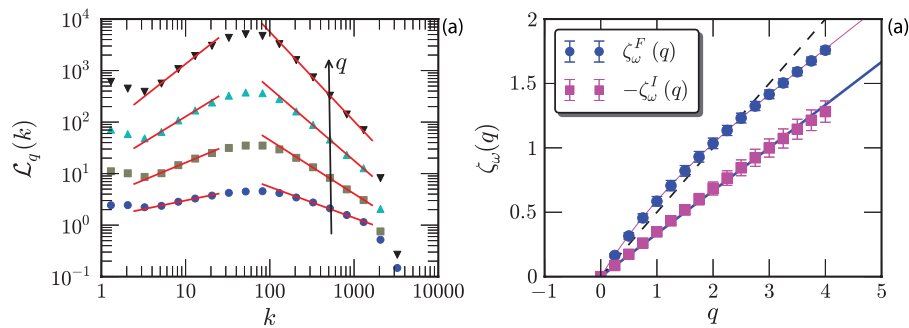


FIG. 7. (a) Measured q th-order Hilbert spectra $\mathcal{L}_q(k)$ for $q = 1, 2, 3, 4$. Power-law behavior is observed on the range $200 \leq k \leq 2000$ for the forward enstrophy cascade and on the range $3 \leq k \leq 20$ for the inverse energy cascade, respectively. The scaling exponents $\zeta_\omega(q)$ are then estimated on this dual power-law ranges. (b) Measured scaling exponents $\zeta_\omega^F(q)$ (\circ) and $-\zeta_\omega^I(q)$ (\square). For comparison, the dashed line is $q/3$ and the solid line is for a log-Poisson fitting $\zeta_\omega^F(q) = q/3 + 0.45(1 - 0.43^q)$. The errorbar indicates 95% fitting confidence.

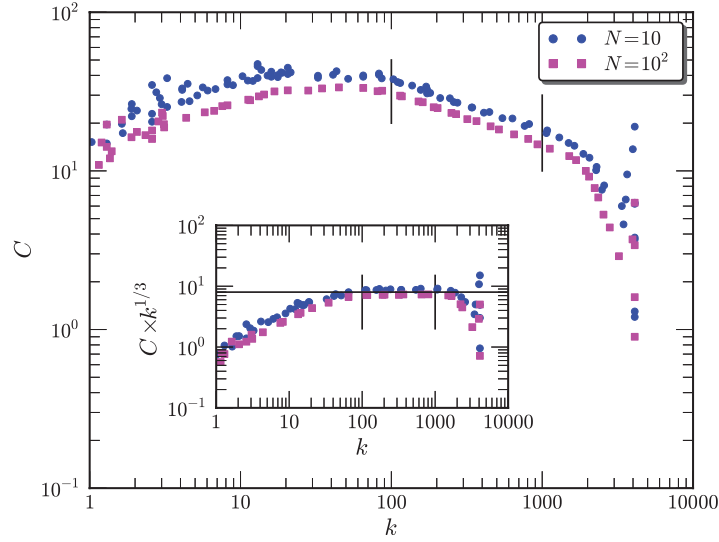


FIG. 8. Experimental contour line for $N = 10$ (\circ) and $N = 100$ (\square). Power-law behavior is observed on the range $100 \leq k \leq 1000$ with a scaling exponent $\simeq 1/3$. The inset shows the compensated curve by multiplying $k^{1/3}$. The observed power-law indicates an asymptotic scaling exponent $\lim_{q \rightarrow +\infty} \zeta_{\omega}^F(q) = q/3$.

a log-Poisson-like model for the observed scaling exponent, i.e.,

$$\zeta_{\omega}^F(q) = \gamma q + \mathcal{B}(1 - \varphi^q), \quad (17)$$

in which the parameters $\gamma = 1/3$, $\mathcal{B} = 0.45$, and $\varphi = 0.43$ are determined as following. For large value of q (if the corresponding statistics exists), the q th-order Hilbert moments $\mathcal{L}_q(k)$ is thus dominated by the tail of the pdf $p(C, k)$. Therefore, if the scaling behavior holds, the measured joint pdf $p(C, k)$ should also show a scaling behavior for the contour line. We extract the measured contour line for $p(C, k)$ (in points) with two values $N = 10$ (\circ) and 100 (\square), see Fig. 8. Power-law behavior is indeed observed as expected on the range $100 \leq k \leq 2000$. The scaling exponent is found to be $\simeq 1/3$. To emphasize the observed $1/3$ scaling, the compensated curves $C(k)k^{1/3}$ are shown as inset of Fig. 8. A clear plateau is observed on the expected range $100 \leq k \leq 2000$. This yields $\gamma = 1/3$. The rest of the parameters \mathcal{B} and φ are then obtained by using a least square fitting algorithm.

B. Extended self-similarity of structure-functions

As we have shown above that due to the large-scale structure influence the second-order SF fails to identify the power-law behavior of the forward enstrophy cascade, see Fig. 3(b). Here we apply the Extended Self-Similarity (ESS) technique to extract the relative scaling exponents.⁴⁶ Note that for the forward enstrophy cascade, the second-order Hilbert moments provide a scaling exponent $\zeta_{\omega}^F(2) \simeq 1$ and the Fourier power spectrum provides $\beta \simeq 2$. Therefore, we define the ESS of the SFs by using the second-order SFs, i.e.,

$$S_q(\ell) \sim (S_2(\ell))^{\zeta_{\omega}^E(q)}, \quad (18)$$

in which $S_q(\ell) = \langle |\Delta_{\ell} \omega|^q \rangle$, and $\zeta_{\omega}^E(q)$ is the ESS scaling exponent. Figure 9(a) shows the measured pdf of the vorticity increment for different separation scales in the forward enstrophy cascade. Except for $\ell = 0.005$, all the pdfs have an exponential tail and almost collapse with each other. Figure 9(b) shows the ESS plots on the range $0.0005 < \ell < 0.005$, corresponding to a wavenumber range $200 < k < 2000$, which is the scaling range of the forward enstrophy cascade predicted by the Hilbert method. Power-law behavior is observed for all q we considered here. The ESS scaling is estimated on this range by using a least square fitting algorithm. Figure 10(a) shows the measured ESS scaling exponent $\zeta_{\omega}^E(q)$ (\square), in which the errorbar indicates the 95% fitting confidence. For comparison, the scaling exponent provided by the Hilbert method (\circ) is also shown. Graphically, the measured

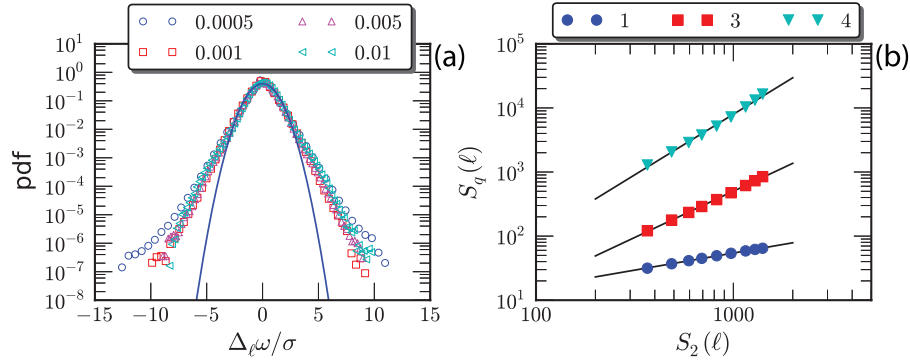


FIG. 9. (a) Measured pdf for vorticity increments with several separation scales ℓ in the range of the forward enstrophy cascade. The Gaussian distribution is illustrated by a solid line. Note that except for the first scale ($\ell = 0.0005$), they all have an exponential tails and do collapse with each other. (b) Extended Self-Similarity plots of the SFs on the range $0.0005 < \ell < 0.005$, corresponding to a wavenumber range $200 < k < 2000$. The solid line is a power-law fitting on this range by using a least square algorithm. For display clarity, these curves have been vertically shifted.

$\zeta_\omega^E(q)$ indicates a less intermittent vorticity field. To emphasize this point, the singularity spectrum $f_\omega(\alpha)$ is then calculated, i.e.,

$$\alpha_\omega = \zeta_\omega(q)', \quad f_\omega(\alpha) = \min \{ \alpha_\omega q - \zeta_\omega(q) + 1 \}, \quad (19)$$

in which the scaling exponents $\zeta_\omega(q)$ could be either scaling exponent from Hilbert method or one from the SFs. Figure 10(b) shows the measured $f_\omega(\alpha)$ for the forward enstrophy cascade, in which the log-Poisson fitting is illustrated by a solid line. It confirms again that the SFs predict a less intermittent vorticity field.

C. Discussion

Several works have been reported for the forward enstrophy cascade that the Fourier power spectrum of vorticity field possesses a “−2” power-law behavior rather than “−1” one required by Kraichnan’s theory, see Eq. (3). However, there is no theory explanation for this contradiction. Specifically for the Hilbert method, we note that the second-order statistics $\mathcal{L}_2(k)$ provides $\zeta_\omega^F(2) \simeq 1.0$ (respectively “−2.0” for the Hilbert energy spectrum) rather than 0 required by the dimensional argument. The high-order scaling exponents $\zeta_\omega(q)$ provided by the Hilbert method for both the inverse energy cascade and forward enstrophy cascade disagree with the Kraichnan’s theory prediction, see Eq. (16).^{7,22} Furthermore, they do not agree with the logarithmic correction

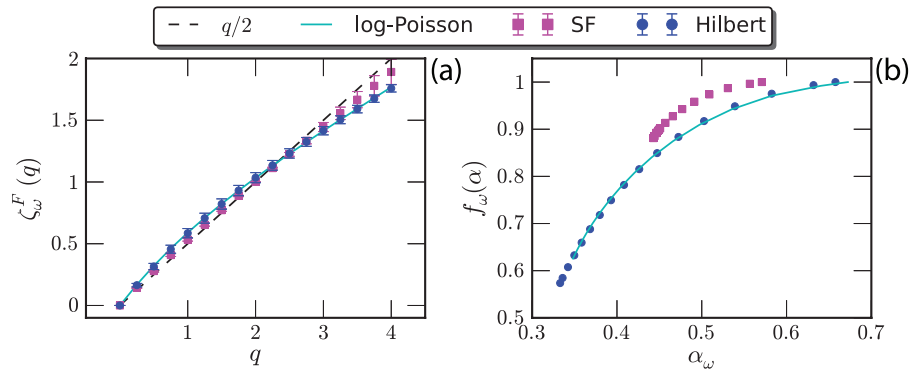


FIG. 10. (a) Comparison of the measured relative scaling exponents $\zeta_\omega^F(q)$ for the SFs (\square), the scaling exponent $\zeta_\omega^F(q)$ provided by the Hilbert method (\circ), and the log-Poisson fitting (solid line). (b) The corresponding singularity spectrum $f_\omega(\alpha)$.

theory either.⁷ It suggests that a new theory is required in future to interpret the vorticity field of 2D turbulence to take into account not only this inconsistency but also the intermittent effect.

We emphasize here that the scaling property of the forward enstrophy cascade might depend on the Ekman friction, the parameter α .^{20,21,25} Therefore, more data sets should be certainly investigated in future to see whether the scaling behavior reported in this work is universal for different α .

V. CONCLUSION

In summary, we have applied the Hilbert methodology to the vorticity field obtained from a high resolution DNS of 2D turbulence. A dual-cascade with almost one decade scales for the inverse energy cascade and forward enstrophy cascade is identified. The scaling exponents $\zeta_\omega(q)$ are extracted. In the inverse energy cascade, the pdf $p(C, k)$ is collapsed with each other with an exponential tail. This indicates a nonintermittent cascade process, which is confirmed by the measured scaling exponent $\zeta_\omega^I(q) = -q/3$. In the forward enstrophy cascade, the measured pdf $p(C, k)$ has also an exponential tail. However, due to the different shape of the core part, they cannot collapse with each other, indicating an intermittent forward enstrophy cascade. The measured scaling exponent $\zeta_\omega^F(q)$ is nonlinear with q when $q \leq 2$, showing intermittency. A log-Poisson fitting, i.e., $\zeta_\omega^F(q) = q/3 + 0.45(1 - 0.43^q)$, is thus proposed to characterize the measured $\zeta_\omega^F(q)$.

ACKNOWLEDGMENTS

This work is sponsored by the National Natural Science Foundation of China under Grant Nos. 11072139, 11032007, 11161160554, 11202122, 11272196, and 11332006, “Pu Jiang” project of Shanghai (Grant No. 12PJ1403500), and the Shanghai Program for Innovative Research Team in Universities. We thank Professor G. Boffetta for providing us the DNS data, which are freely available from the iCFDdatabase.⁴⁷ Y.H. thanks Professor L. Biferale and Professor G. Falkovich for useful discussions and comments. We thank Dr. Gabriel Rilling and Professor Patrick Flandrin from laboratoire de Physique, CNRS & ENS Lyon (France) for sharing their EMD code with us.⁴⁸ We also thank the anonymous referees for their useful comments and suggestions.

- ¹ R. Kraichnan and D. Montgomery, “Two-dimensional turbulence,” *Rep. Prog. Phys.* **43**, 547 (1980).
- ² P. Tabeling, “Two-dimensional turbulence: A physicist approach,” *Phys. Rep.* **362**, 1–62 (2002).
- ³ H. Kellay and W. Goldburg, “Two-dimensional turbulence: a review of some recent experiments,” *Rep. Prog. Phys.* **65**, 845 (2002).
- ⁴ G. Boffetta and R. Ecke, “Two-dimensional turbulence,” *Annu. Rev. Fluid Mech.* **44**, 427–451 (2012).
- ⁵ F. Bouchet and A. Venaille, “Statistical mechanics of two-dimensional and geophysical flows,” *Phys. Rep.* **515**, 227–295 (2012).
- ⁶ R. Irion, “Soap films reveal whirling worlds of turbulence,” *Science* **284**, 1609–1610 (1999).
- ⁷ G. Falkovich and V. Lebedev, “Universal direct cascade in two-dimensional turbulence,” *Phys. Rev. E* **50**, 3883 (1994).
- ⁸ S. Chen, R. Ecke, G. Eyink, X. Wang, and Z. Xiao, “Physical mechanism of the two-dimensional enstrophy cascade,” *Phys. Rev. Lett.* **91**, 214501 (2003).
- ⁹ S. Chen, R. Ecke, G. Eyink, M. Rivera, M. Wan, and Z. Xiao, “Physical mechanism of the two-dimensional inverse energy cascade,” *Phys. Rev. Lett.* **96**, 084502 (2006).
- ¹⁰ G. Boffetta and S. Musacchio, “Evidence for the double cascade scenario in two-dimensional turbulence,” *Phys. Rev. E* **82**, 016307 (2010).
- ¹¹ A. Alexakis and C. Doering, “Energy and enstrophy dissipation in steady state 2D turbulence,” *Phys. Lett. A* **359**, 652–657 (2006).
- ¹² H. Xia, D. Byrne, G. Falkovich, and M. Shats, “Upscale energy transfer in thick turbulent fluid layers,” *Nat. Phys.* **7**, 321–324 (2011).
- ¹³ H. Xia, H. Punzmann, G. Falkovich, and M. Shats, “Turbulence-condensate interaction in two dimensions,” *Phys. Rev. Lett.* **101**, 194504 (2008).
- ¹⁴ T. Tran, P. Chakraborty, N. Guttenberg, A. Prescott, H. Kellay, W. Goldburg, N. Goldenfeld, and G. Gioia, “Macroscopic effects of the spectral structure in turbulent flows,” *Nat. Phys.* **6**, 438–441 (2010).
- ¹⁵ D. Kelley and N. Ouellette, “Spatiotemporal persistence of spectral fluxes in two-dimensional weak turbulence,” *Phys. Fluids* **23**, 115101–115101 (2011).
- ¹⁶ S. Merrifield, D. Kelley, and N. Ouellette, “Scale-dependent statistical geometry in two-dimensional flow,” *Phys. Rev. Lett.* **104**, 254501 (2010).
- ¹⁷ A. Celani, S. Musacchio, and D. Vincenzi, “Turbulence in more than two and less than three dimensions,” *Phys. Rev. Lett.* **104**, 184506 (2010).

- ¹⁸ N. Khurana and N. Ouellette, "Interactions between active particles and dynamical structures in chaotic flow," *Phys. Fluids* **24**, 091902–091902 (2012).
- ¹⁹ G. Van Heijst and H. Clercx, "Laboratory modeling of geophysical vortices," *Annu. Rev. Fluid Mech.* **41**, 143–164 (2009).
- ²⁰ G. Boffetta, A. Celani, S. Musacchio, and M. Vergassola, "Intermittency in two-dimensional Ekman-Navier-Stokes turbulence," *Phys. Rev. E* **66**, 026304 (2002).
- ²¹ G. Boffetta, "Energy and enstrophy fluxes in the double cascade of two-dimensional turbulence," *J. Fluid Mech.* **589**, 253–260 (2007).
- ²² R. Kraichnan, "Inertial ranges in two-dimensional turbulence," *Phys. Fluids* **10**, 1417–1423 (1967).
- ²³ U. Frisch, *Turbulence: The Legacy of AN Kolmogorov* (Cambridge University Press, 1995).
- ²⁴ Y. Huang, F. Schmitt, Z. Lu, P. Fougairolles, Y. Gagne, and Y. Liu, "Second-order structure function in fully developed turbulence," *Phys. Rev. E* **82**, 026319 (2010).
- ²⁵ L. Biferale, M. Cencini, A. Lanotte, and D. Vergni, "Inverse velocity statistics in two-dimensional turbulence," *Phys. Fluids* **15**, 1012–1020 (2003).
- ²⁶ H. Kellay, X. Wu, and W. Goldburg, "Vorticity measurements in turbulent soap films," *Phys. Rev. Lett.* **80**, 277–280 (1998).
- ²⁷ J. Paret, M. Jullien, and P. Tabeling, "Vorticity statistics in the two-dimensional enstrophy cascade," *Phys. Rev. Lett.* **83**, 3418–3421 (1999).
- ²⁸ K. Nam, E. Ott, T. Antonsen, Jr., and P. Guzdar, "Lagrangian chaos and the effect of drag on the enstrophy cascade in two-dimensional turbulence," *Phys. Rev. Lett.* **84**, 5134–5137 (2000).
- ²⁹ D. Bernard, "Influence of friction on the direct cascade of the 2D forced turbulence," *Europhys. Lett.* **50**, 333 (2000).
- ³⁰ Y. Tsang, E. Ott, T. Antonsen, Jr., and P. Guzdar, "Intermittency in two-dimensional turbulence with drag," *Phys. Rev. E* **71**, 066313 (2005).
- ³¹ G. Falkovich and V. Lebedev, "Vorticity statistics in the direct cascade of two-dimensional turbulence," *Phys. Rev. E* **83**, 045301 (2011).
- ³² G. Falkovich and K. R. Sreenivasan, "Lessons from hydrodynamic turbulence," *Phys. Today* **59**, 43 (2006).
- ³³ Y. Huang, F. Schmitt, Z. Lu, and Y. Liu, "An amplitude-frequency study of turbulent scaling intermittency using Hilbert spectral analysis," *Europhys. Lett.* **84**, 40010 (2008).
- ³⁴ Y. Huang, F. Schmitt, J.-P. Hermand, Y. Gagne, Z. Lu, and Y. Liu, "Arbitrary-order Hilbert spectral analysis for time series possessing scaling statistics: Comparison study with detrended fluctuation analysis and wavelet leaders," *Phys. Rev. E* **84**, 016208 (2011).
- ³⁵ N. E. Huang, Z. Shen, S. R. Long, M. C. Wu, H. H. Shih, Q. Zheng, N. Yen, C. C. Tung, and H. H. Liu, "The empirical mode decomposition and the Hilbert spectrum for nonlinear and non-stationary time series analysis," *Proc. R. Soc. London, Ser. A* **454**, 903–995 (1998).
- ³⁶ N. E. Huang, Z. Shen, and S. R. Long, "A new view of nonlinear water waves: The Hilbert Spectrum," *Annu. Rev. Fluid Mech.* **31**, 417–457 (1999).
- ³⁷ P. Flandrin and P. Gonçalves, "Empirical mode decompositions as data-driven Wavelet-like expansions," *Int. J. Wavelets, Multires. Info. Proc.* **02**, 477–496 (2004).
- ³⁸ G. Rilling, P. Flandrin, and P. Gonçalves, "On empirical mode decomposition and its algorithms," in *Proceedings of the IEEE-EURASIP Workshop on Nonlinear Signal and Image Processing* (IEEE, 2003).
- ³⁹ Y. Huang, "Arbitrary-order Hilbert spectral analysis: Definition and application to fully developed turbulence and environmental time series," Ph.D. thesis, Université des Sciences et Technologies de Lille – Lille 1, France, and Shanghai University, China, 2009.
- ⁴⁰ L. Cohen, *Time-Frequency Analysis* (Prentice Hall PTR Englewood Cliffs, NJ, 1995).
- ⁴¹ P. Flandrin, *Time-Frequency/Time-Scale Analysis* (Academic Press, 1998).
- ⁴² Y. Huang, L. Biferale, E. Calzavarini, C. Sun, and F. Toschi, "Lagrangian single particle turbulent statistics through the Hilbert-Huang transforms," *Phys. Rev. E* **87**, 041003(R) (2013).
- ⁴³ C. Pasquero and G. Falkovich, "Stationary spectrum of vorticity cascade in two-dimensional turbulence," *Phys. Rev. E* **65**, 056305 (2002).
- ⁴⁴ P. A. Davidson and B. R. Pearson, "Identifying turbulent energy distribution in real, rather than fourier, space," *Phys. Rev. Lett.* **95**, 214501 (2005).
- ⁴⁵ F. Toschi, L. Biferale, G. Boffetta, A. Celani, B. Devenish, and A. Lanotte, "Acceleration and vortex filaments in turbulence," *J. Turbul.* **6**, N15 (2005).
- ⁴⁶ R. Benzi, S. Ciliberto, R. Tripiccone, C. Baudet, F. Massaioli, and S. Succi, "Extended self-similarity in turbulent flows," *Phys. Rev. E* **48**, R29–R32 (1993).
- ⁴⁷ See <http://cfd.cineca.it> for public DNS database of the two-dimensional turbulence.
- ⁴⁸ See <http://perso.ens-lyon.fr/patrick.flandrin/emd.html> for website for Empirical Mode Decomposition Matlab codes.